AIAA JOURNAL
Vol. 42, No. 4, April 2004

Finite Element Modal Formulation for Hypersonic Panel Flutter Analysis with Thermal Effects

Guangfeng Cheng* and Chuh Mei†
Old Dominion University, Norfolk, Virginia 23529-0247

A finite element time-domain modal formulation for analyzing nonlinear flutter of panels subjected to hypersonic airflow has been developed. Von Kármán large deflection plate theory is used for description of the structural nonlinearity, and third-order piston theory is employed to consider the aerodynamic nonlinearity. The thermal loadings of uniformly distributed surface temperatures and temperature gradients through the panel thickness are considered. By the application of the modal truncation technique, the number of governing equations of motion is reduced dramatically so that the computational costs are reduced significantly. All possible types of panel behavior, including flat and stable, buckled but dynamically stable, limit cycle oscillation (LCO), periodic motion, and chaotic motion were observed. Examples of the applications of the proposed methodology were flutter responses of isotropic and composite panels. Special emphasis was placed on the boundary between LCO and chaos and on the route to chaos. Time history, phase plane plot, Poincaré map, bifurcation diagram, and Lyapunov exponent are employed in the chaos study. It is found that at low or moderately high dynamic pressures, the fluttering panel typically takes a period-doubling route to evolve into chaos, whereas, at high dynamic pressures, the route generally involves bursts of chaos and rejuvenations of periodic motions.

Nomenclature

$[A_a]$, $[A1]$, $[A2]$	=	linear, first- and second-order aerodynamic influence matrices
$[\bar{A}]$	=	modal aerodynamic influence matrix
C_a	=	aerodynamic damping coefficient
$[G]$, $[G1]$, $[G2]$	=	linear, first- and second-order aerodynamic damping matrices
$[\bar{G}]$	=	modal aerodynamic damping matrix
g_a	=	nondimensional aerodynamic damping
$[K_0]$, $[K1]$, $[K2]$	=	linear, first- and second-order stiffness matrices
$[\bar{K}]$	=	modal linear stiffness matrix
M_r	=	flow parameter, $M_\infty(h/a)$
M_∞	=	freestream Mach number
$[M]$	=	mass matrix
$[\bar{M}]$	=	modal mass matrix
$\{P\}$	=	force vector
p_a	=	aerodynamic pressure
p_∞	=	undisturbed pressure
q	=	dynamic pressure
$\{q\}$	=	modal coordinate vector
r	=	panel thickness-width ratio, h/a
T_0	=	average temperature
T_1	=	temperature gradient across panel thickness
V	=	airflow velocity
$\{W\}$	=	panel structural node displacement vector
$\{X\}$	=	state vector
γ	=	ratio of specific heat, 1.4
Δ	=	incremental value
λ	=	nondimensional dynamic pressure
$[\Phi]$	=	modal matrix
$\{\phi\}$	=	eigenvector
ω	=	frequency

Subscripts

a	=	air
b	=	bending
cr	=	critical
m	=	membrane/composite matrix
Nb	=	stiffness matrices due to $\{N_b\}$
NL	=	nonlinear
Nm	=	stiffness matrices due to $\{N_m\}$
$N\Delta T$	=	stiffness matrices due to $\{N_{\Delta T}\}$
ΔT	=	thermal

Received 23 December 2002; presented as Paper 2003-1517 at the AIAA/ASME/ASCE/AHS/ASC 44th Structures, Structural Dynamics, and Materials Conference, Norfolk, VA, 7–10 April 2003; revision received 15 October 2003; accepted for publication 15 October 2003.

*Postdoctoral Fellow, Aerospace Engineering. Member AIAA.
†Professor, Aerospace Engineering. Associate Fellow AIAA.

Introduction

THEORETICAL and experimental studies of panel flutter began in the 1950s. Reviews of the findings from such early stage research were summarized by Fung[1] and Johns.[2,3] In a later survey by Dowell,[4] a voluminous theoretical literature on panel flutter was grouped into four basic categories based on the structural and aerodynamic theories employed, as shown in Table 1. Table 1 is taken from a recent review paper by Mei et al.[5] with the addition of a type 6 analysis in this paper. Augmentation of the fifth type of analysis was attributed to Gray and Mei[6] on consideration of hypersonic panel flutter analysis theory proposed by McIntosh.[7]

For the type 5 nonlinear panel flutter analysis, nonlinearities involved with panel flutter arise from two aspects: the structural and aerodynamic points of view. Material nonlinearity was not considered. For flight vehicles operating in the hypersonic regime, unsteady nonlinear aerodynamic theories are more applicable to the problem. Aerodynamic nonlinearity was first considered in conjunction with structural nonlinearity by McIntosh[7,8] and Eastep and McIntosh[9] in flutter analysis of simply supported two- and three-dimensional panels in hypersonic airflow. Two nonlinear aerodynamic terms, $(\partial w/\partial x)^2$ and $[(\partial w/\partial x)(\partial w/\partial t)]$, taken from the third-order piston theory, were added to the linear piston theory to address the aerodynamic nonlinearity. The Rayleigh–Ritz approximation was employed in a modal representation of the panel transverse deflection. The nonlinear modal equations of motion were then integrated in the time domain until the observation of limit cycle oscillation (LCO). Major findings include 1) the two nonlinear

Table 1 Panel flutter analysis categories

Type	Structure theory	Aerodynamic theory	Range of Mach no.
1	Linear	Linear piston	$\sqrt{2} < M_\infty < 5$
2	Linear	Linearized potential flow	$1 < M_\infty < 5$
3	Nonlinear	Linear piston	$\sqrt{2} < M_\infty < 5$
4	Nonlinear	Linearized potential flow	$1 < M_\infty < 5$
5	Nonlinear	Nonlinear piston	$M_\infty > 5$
6	Nonlinear	Euler or Navier–Stokes equations	Transonic, supersonic, hypersonic

terms proved to be the most important sources of aerodynamic nonlinearity, 2) the nonlinear aerodynamic loading introduced a bias of panel motion toward the cavity that could be attributed to the overpressurization effects of the additional nonlinear pressure terms, 3) aerodynamic loading has no effects on limit cycle frequency and little effect on panel stress, and 4) contrary to the stabilizing effect from the structural nonlinear membrane stress on panel motion, nonlinear aerodynamic loading plays a destabilizing role. The interplay between these two mechanisms distinguishes panel flutter at hypersonic speeds from that at supersonic speeds. For some system parameters, aerodynamic nonlinearities decrease the critical dynamic pressure for panel flutter and, hence, produce a soft spring effect on the prediction of the stability boundary. A rather later study on two-dimensional panel flutter in hypersonic flow by Gray and Mei[10] using a finite element method confirmed conclusions 1, 2, and 4. The third-order piston theory was used for aerodynamic pressure, and the significance of each of the nonlinear terms was investigated in detail. Gray and Mei[10] developed the linearized updated mode with nonlinear time function (LUM/NTF) approximation method, which is a generic finite element frequency-domain LCO solver. The same solution procedure was then extended to panel flutter analysis of three-dimensional composite panels at hypersonic speeds in their later work.[6] Effects of panel support conditions, panel thickness-to-length ratio, panel aspect ratio, and number of laminate layers on LCO amplitude were studied. Good agreement between the flutter analysis by the proposed finite element frequency-domain approach and the existing analytical methods was found.

Other contributions on hypersonic panel flutter have been made by several teams of investigators. Bein et al.[11] studied the flutter of simply support curved shallow orthotropic panels with uniform temperature distribution due to aerodynamic heating. Coupled nonlinear panel flutter modal equations were obtained using partial differential equation (PDE)/Galerkin's method, and direct time numerical integration was conducted to compute the LCO amplitudes. The unsteady aerodynamic pressure distribution from third-order piston theory was compared to that from the solutions of Euler equations, and good agreement was found. Nydick et al.[12] continued the study of hypersonic flutter of curved panels by consideration of more comprehensive temperature distributions, presence of shocks in the flow, and an alternative representation of aerodynamic loading. (Temperature is a function of all three coordinates, x, y and z.) The unsteady aerodynamic pressure was obtained by third-order piston theory, and it was compared with those obtained from the Euler equations and from the Navier–Stokes equations in light of the viscosity presented in practical hypersonic flowfields. The comparisons showed that the third-order piston theory compared very well with the unsteady aerodynamic pressure from the unsteady Euler equations; however, the Navier–Stokes solutions predict a much lower (up to 60% lower) surface pressure than the Euler equations and piston theory. However, the LCO amplitudes obtained by Nydick et al. compared well with the results by Gray and Mei[6] for the case of hypersonic flutter of orthotropic panels. The most recent work by Thuruthimattam et al.[13] further extended hypersonic flutter analysis to a double-wedge airfoil and a three-dimensional generic hypersonic vehicle. The flutter analysis was conducted on the basis of an integrated procedure that couples the computational fluid dynamics solution with structural finite element analysis. Euler and Navier–Stokes aerodynamics were primarily used for the aerodynamic loading. However, the aeroelastic responses were validated by comparison with results from an independently developed aeroelastic code based on third-order piston theory. It was concluded that, in a large portion of the flight envelope, good agreement is found between the double-wedge airfoil flutter responses from calculations based on piston theory and those from Euler solutions. Only in certain portions of the flight envelope were significant differences observed between Euler based results and Navier–Stokes based solutions. For the three-dimensional generic hypersonic vehicle model, the difference between viscous (Navier–Stokes) and inviscid (Euler, piston) solutions on the vehicle is substantially smaller than on the double-wedge airfoil.

Nonlinear panel flutter considering aerodynamic nonlinearity was studied by Chandiramani et al.[14,15] and Chandiramani and Librescu.[16] High-order shear deformation theory and the third-order piston theory were used, and the panel flutter modal equations were derived using Galerkin's method. The arc length continuation method was used to determine the static equilibrium state, and its dynamic stability was subsequently examined. Effects of small geometrical panel imperfection, airflow direction, and uniform in-plane compression on flutter boundary were investigated. It was concluded that for moderately thick composite panel, shear deformation theory and nonlinear aerodynamic theory are required for determination of the flutter boundary. The postflutter motion of such composite panels was also investigated by applying a predictor together with a Newton–Raphson-type corrector technique for periodic solution and numerical integration for quasi-periodic or chaotic flutter solutions. Results showed that edge constraints normal to the flow appear to stabilize the panel, whereas those parallel to the flow do not noticeably affect the flutter speed and the immediate postcritical response. For geometrically imperfect panels, chaotic motions via the period-doubling scenario were obtained. For perfect panels, a sudden transition from the buckled state to chaos, followed by complicated periodic motion, occurred. The near critical point bifurcation behavior of a simply supported isotropic panel was studied by Sri Namachchivaya and Lee.[17] Third-order piston theory and Galerkin's method were employed. It was found that nonlinear aerodynamic terms could completely change the bifurcation behavior of the panel.

The applicability of various hypersonic aerodynamic theories is still a subject of active research. One effort made by Chen and Liu,[18] Chavez and Liu,[19] and Liu et al.[20] was to develop a unified method for computation of the flowfield of hypersonic/supersonic airflow that could be applied to aeroelastic problems. Two methods, the perturbed Euler characteristics (PEC) method and the unified hypersonic/supersonic lifting surface method, were developed. The PEC method is virtually an Euler approximation to the hypersonic flow. The method is developed to account for the effects of unsteady Mach wave/shock wave interaction so that the rotationality and body thickness effects are considered. The lifting surface method is intended to generalize the exact three-dimensional linear theory for treatments of lifting surfaces in unsteady supersonic flow[18] and to include the effects of wing thickness and upstream influence in a unified supersonic/hypersonic flow regime. Both methods are proposed for panel flutter applications to extend the applicable range of piston theory. However, there are no sound proofs that either of the two methods could supersede the piston theory at present. As indicated by Liu et al.,[20] because of the limitation in available measured data, further validation and applicability assessment of the proposed method are warranted.

Another concern, from the fluid mechanics point of view, is the influence of boundary layers on panel flutter. Analysis and experimental reports on turbulent boundary-layer effects can be dated back to the early years of flutter study.[21–23] It was found that the turbulent boundary layer has a significant effect on the flutter boundary of panels at low supersonic Mach numbers. The effect decreases rapidly with increasing Mach number. Recently, Gordnier and Visbal[24,25] developed a three-dimensional viscous aeroelasticity

solver that couples the full-fidelity Navier–Stokes equations with a finite difference procedure for von Kármán plate equations. A subiteration strategy was used to eliminate lagging errors between the fluid motions and structural solvers. Boundary-layer influences on three-dimensional nonlinear panel flutter were then investigated using the new aeroelastic solver. Again, it is found that only at low supersonic or subsonic Mach number does viscosity have significant effects on panel flutter. It was also suggested by Crandall and Zhu[26] that the boundary-layer pressure fluctuations should be treated as a random structural vibration problem so that the panel failure may be due to acoustic fatigue rather than panel flutter.

The influence of acoustic pressure on supersonic nonlinear flutter of composite panels was studied by Abdel-Motagaly et al.[27] using a finite element modal formulation with time numerical integration. They concluded that, at low ($\lambda \ll \lambda_{cr}$) dynamic pressure, only acoustic excitations (acoustic fatigue) are to be considered, whereas at significant (but $\lambda < \lambda_{cr}$) and high ($\lambda > \lambda_{cr}$) dynamic pressures both acoustic and aerodynamic pressures have to be considered. Analysis comparisons among panel flutter LCO results from Euler flow theory, linear potential flow theory, and quasi-steady supersonic theory were recently made by Selvam et al.[28] The Euler equations are solved numerically for aerodynamic pressure with an implicit approximately factored finite difference algorithm. Panel governing equations of motion based on von Kármán large deflection plate theory are solved with the Newmark–beta integration scheme for flutter response. Newton-like subiteration is employed to eliminate the lagging errors associated with exchange of pressure and deformations between airflow and the panel. The LCO results showed that for given LCO amplitude, the difference among the required dynamic pressure values is around 5%.

In summary, the Euler aerodynamics (or its variations) and piston theory are applicable for unsteady, inviscid flow, and Navier–Stokes equations for viscous fluids. Good agreement exists between panel flutter analyses using Euler equations and by piston theory.[12,28] For panel flutter at hypersonic flow, viscosity effects can be neglected and nonlinear aerodynamic theory must be employed.[12] This gives the reason for applying the third-order piston theory in the present study of panel flutter of composite panels in hypersonic flow.

In the existing literature, there are mainly three types of methods applied to hypersonic panel flutter analysis: analytical PDE/Galerkin approach, finite element frequency-domain method, and finite element time-domain method. The analytical approach has intrinsic limitations on dealing with complicated boundary conditions and anisotropic material properties. The finite element frequency-domain method can only study the LCO behavior. The major obstacles to implementation of the finite element time-domain formulation in structure node degrees of freedom (DOF) include[29,30] 1) the large number of DOF that result in large number of equations to solve, 2) the nonlinear stiffness matrices that have to be assembled and updated from the element nonlinear stiffness matrices at each time step, and 3) the time step of integration that has to be extremely small. Zhou et al.[31] presented a finite element time-domain modal formulation for nonlinear supersonic panel flutter analysis. The time-domain modal formulation is extended to flutter analysis of panels at hypersonic airflow in present study for the first time.

Finite Element Formulation

The panel is subjected in a combined environment of aerodynamic flow and thermal exposure. High-temperature and hypersonic airflow can cause large-amplitude vibration of the panel. Von Kármán large deflection plate theory is herein employed to describe the nonlinear strain and displacement relationships. The third-order piston theory[32] is used for aerodynamic pressure distribution:

$$\Delta p = p_a - p_\infty = (2q/M_\infty)\Big\{(1/V)C_{1t}w_{,t} + C_{1x}w_{,x} + [(\gamma+1)/4]M_\infty[(1/V)C_{2t}w_{,t} + C_{2x}w_{,x}]^2 + [(\gamma+1)/12]M_\infty^2[(1/V)C_{3t}w_{,t} + C_{3x}w_{,x}]^3\Big\} \tag{1}$$

where C are parameters of 0 or 1 for evaluating the influence of each of the nonlinear aerodynamic terms.

For thin-walled structures that have extensive applications in aerospace, the steady-state temperature field is a function of all three coordinates, that is, $\Delta T(x, y, z)$. The temperature variation is herein assumed to be linearly distributed across the plate thickness as $\Delta T = T_0 + zT_1/h$, where T_0 is the average temperature rise of the plate and T_1 is the temperature gradient through the plate thickness. When $T_1 = 0.0$ is set, a special case of uniform temperature distribution is reached.

The 24-DOF Bogner–Fox–Schmit (BFS) C^1 conforming rectangular plate element is used and extended for the finite element model. The governing equation of motion (EOM) is derived using the principle of virtual work. The system equation of motion in physical coordinates, that is, structural degree of freedom, can be written as[6,33]

$$\frac{1}{\omega_0^2}\begin{bmatrix} M_b & 0 \\ 0 & M_m \end{bmatrix}\begin{Bmatrix} \ddot{W}_b \\ \ddot{W}_m \end{Bmatrix} + \frac{g_a}{\omega_0}\begin{pmatrix} [G] + [G1_t] + [G2_{bt}] + [G2_t] & 0 \\ 0 & 0 \end{pmatrix} \times \begin{Bmatrix} \dot{W}_b \\ \dot{W}_m \end{Bmatrix} + \left[\lambda\begin{pmatrix} [A_a] + [A1_t] + [A1_b] + [A2_{bt}] + [A2_b] & 0 \\ 0 & 0 \end{pmatrix} + \begin{bmatrix} K_b & K_{bm} \\ K_{mb} & K_m \end{bmatrix} - \begin{bmatrix} K_{N\Delta T} & 0 \\ 0 & 0 \end{bmatrix} + \begin{pmatrix} [K1_{Nm}] + [K1_{Nb}] & [K1_{bm}] \\ [K1_{mb}] & 0 \end{pmatrix} + \begin{bmatrix} K2 & 0 \\ 0 & 0 \end{bmatrix}\right]\begin{Bmatrix} W_b \\ W_m \end{Bmatrix} = \begin{Bmatrix} P_{b\Delta T} \\ P_{m\Delta T} \end{Bmatrix} \tag{2a}$$

or simply

$$\left(1/\omega_0^2\right)[M]\{\ddot{W}\} + (g_a/\omega_0)[G_{NL}]\{\dot{W}\} + (\lambda[A_{NL}] + [K_0] - [K_{N\Delta T}] + [K1] + [K2])\{W\} = \{P_{\Delta T}\} \tag{2b}$$

The expansion theorem states that any possible motion of the system can be described as a linear combination of the modal vectors. Therefore, the deflection of the panel can be assumed as

$$\{W\} = \begin{Bmatrix} W_b \\ W_m \end{Bmatrix} = \sum_{r=1}^{n} q_r(t)\begin{Bmatrix} \phi_{br} \\ \phi_{mr} \end{Bmatrix} = \sum_{r=1}^{n} q_r(t)\{\phi_r\} = [\Phi]\{q\} \tag{3}$$

When the relationship given in Eq. (3) is applied, the system level EOM in physical coordinates can be transferred into modal coordinates as

$$\left(1/\omega_0^2\right)[\bar{M}]\{\ddot{q}\} + (g_a/\omega_0)[\bar{G}_{NL}]\{\dot{q}\} + (\lambda[\bar{A}_{NL}] + [\bar{K}] + [\bar{K}1] + [\bar{K}2])\{q\} = [\Phi]^T\{P_{\Delta T}\} \tag{4a}$$

where

$$[\bar{M}] = [\Phi]^T[M][\Phi], \qquad [\bar{G}_{NL}] = [\Phi]^T[G_{NL}][\Phi] \tag{4b}$$

$$([\bar{A}_{NL}], [\bar{K}], [\bar{K}1], [\bar{K}2]) = [\Phi]^T([A_{NL}], [K_0] - [K_{N\Delta T}], [K1], [K2])[\Phi] \tag{4c}$$

In Eq. (2), the first- and second-order nonlinear stiffness matrices $[K1]$ and $[K2]$, nonlinear aerodynamic stiffness matrix $[A_{NL}]$, and nonlinear aerodynamic damping matrix $[G_{NL}]$ are dependent on the nodal displacement vectors $\{W_b\}$ or $\{W_m\}$. While transferred into modal coordinates, all these nonlinear matrices are evaluated with modal vectors $\{\phi_r\}$. The first- and second-order nonlinear stiffness matrices, $[K1]$ and $[K2]$, can be evaluated as[31,33]

$$[K1] = \sum_{r=1}^{n} q_r[K1]^{(r)}, \qquad [K2] = \sum_{r=1}^{n}\sum_{s=1}^{n} q_r q_s[K2]^{(rs)} \tag{5}$$

where the superscript r denotes that $\{\phi_r\}$ is used in evaluation of the first-order nonlinear modal stiffness matrix. Similarly, the superscript rs denotes that $\{\phi_r\}$ and $\{\phi_s\}$ are used in evaluation of the second-order nonlinear modal stiffness matrix. The nonlinear modal stiffness matrices, $[K1]^{(r)}$ and $[K2]^{(rs)}$, are constant. The corresponding transformed matrices, $[\bar{K}1]$ and $[\bar{K}2]$, are computed from definitions given in Eq. (4c). Similiar to the evaluation procedure for $[K1]$ and $[K2]$, the nonlinear aerodynamic matrices can be evaluated as[33]

$$[G1_t] = \sum_{r=1}^{n} \dot{q}_r [G1_t]^{(r)} \tag{6a}$$

$$[G2_{bt}] = \sum_{r=1}^{n}\sum_{s=1}^{n} q_r \dot{q}_s [G2_{bt}]^{(rs)} \tag{6b}$$

$$[G2_t] = \sum_{r=1}^{n}\sum_{s=1}^{n} \dot{q}_r \dot{q}_s [G2_t]^{(rs)} \tag{6c}$$

$$[A1_t] = \sum_{r=1}^{n} \dot{q}_r [A1_t]^{(r)} \tag{6d}$$

$$[A1_b] = \sum_{r=1}^{n} q_r [A1_b]^{(r)} \tag{6e}$$

$$[A2_{bt}] = \sum_{r=1}^{n}\sum_{s=1}^{n} q_r \dot{q}_s [A2_{bt}]^{(rs)} \tag{6f}$$

$$[A2_b] = \sum_{r=1}^{n}\sum_{s=1}^{n} q_r q_s [A2_b]^{(rs)} \tag{6g}$$

During the time integration, the modal coordinate q_r and corresponding velocity $\dot{q}_r$ are generated simultaneously; hence, they are available at each time step. Again, the nonlinear modal aerodynamic matrices $[G1_t]^{(r)}$, $[G2_{bt}]^{(rs)}$, $[G2_t]^{(rs)}$, $[A1_t]^{(r)}$, $[A1_b]^{(r)}$, $[A2_{bt}]^{(rs)}$, and $[A2_b]^{(rs)}$ are constant. The corresponding transformed matrices, $[\bar{G}_{\mathrm{NL}}]$ and $[\bar{A}_{\mathrm{NL}}]$, are computed as defined in Eqs. (4b) and (4c).

When the direct integration of Eq. (4a) is performed, many time-integration methods are available,[34] such as the central difference method, the Houbolt method, the Newmark method, etc. Herein, the fourth-order Runge–Kutta method is adopted. Numerical integration is carried out in the state-space form:

$$\{X\} = \begin{Bmatrix} \{X_1\} \\ \{X_2\} \end{Bmatrix} = \begin{Bmatrix} \{q\} \\ \{\dot{q}\} \end{Bmatrix} \tag{7}$$

The state-space representation of governing EOM can be written as

$$\begin{Bmatrix} \{\dot{X}_1\} \\ \{\dot{X}_2\} \end{Bmatrix} = \begin{bmatrix} 0 & [I] \\ -[K_{\mathrm{sys}}] & -[C_{\mathrm{sys}}] \end{bmatrix} \begin{Bmatrix} \{X_1\} \\ \{X_2\} \end{Bmatrix} + \begin{bmatrix} 0 \\ [I] \end{bmatrix} \{F_{\mathrm{sys}}\} \tag{8}$$

in which the system stiffness and damping matrices are defined as

$$[K_{\mathrm{sys}}] = \omega_0^2 [\bar{M}]^{-1} (\lambda[\bar{A}_{\mathrm{NL}}] + [\bar{K}] + [\bar{K}1] + [\bar{K}2]) \tag{9}$$

$$[C_{\mathrm{sys}}] = g_a \omega_0 [\bar{M}]^{-1} [\bar{G}_{\mathrm{NL}}] \tag{10}$$

$$\{F_{\mathrm{sys}}\} = \omega_0^2 [\bar{M}]^{-1} [\Phi]^T \{P_{\Delta T}\} \tag{11}$$

and matrix $[I]$ is the identity matrix.

The system governing EOM [Eq. (4)] is then solved in the time domain through numerical integration for the flutter responses. Various panel behaviors are observed through time histories, phase plane plot, and Poincaré map (see Refs. 35 and 36). Chaos study is conducted by assistance of bifurcation diagram[35] and evaluation of the largest Lyapunov exponent (see Ref. 37). A detailed flowchart that shows the already mentioned solution procedure may be found in Cheng.[33]

Numerical Results

A. Validation of the Finite Element Formulation

To validate the present finite element modal formulation, comparison was made for LCO amplitudes of panel flutter in hypersonic flow between present finite element analysis results, results by Gray and Mei[6] using the frequency-domain LUM/NTF method, and results by Nydick et al.[12] using analytical Galerkin method and numerical integration. The material properties [boron/aluminum (B/Al) and graphite/epoxy (Gr/Ep)] of all panels studied are listed in Table 2. Figure 1 shows the LCO amplitudes for the single-layer B/Al panel (panel 2) and cross-ply B/Al panel (panel 3). It demonstrates that there is good agreement among the three methods.

B. Flutter of Isotropic Panels

Thin panels made of isotropic materials, such as aluminum and its alloys and titanium and its alloys, have earned extensive aerospace applications. Besides their potential high strength and/or light weight, the simplicity of material properties greatly eases the corresponding analysis work. The in-plane boundary conditions for all cases are assumed to be immovable, that is, $u(0, y) = u(a, y) = v(x, 0) = v(x, b) = 0$. Other boundary conditions are possible for the finite element method presented.

A simply supported, square, aluminum panel (panel 1) is investigated. With reference to Dowell[38] and Nydick et al.,[12] eight airflow direction modes, mode (1, 1), (2, 1), . . . , (8, 1) are used and a mesh size of 12×8 (or 96 BFS elements) is adopted. Because of the high nonlinearity inherent with hypersonic panel flutter, chaos becomes inevitable as system control parameters change, that is, changes in temperature and in dynamic pressure. Therefore, observe the route that chaos evolves via bifurcation diagrams. Figures 2 and 3 are examples of bifurcation diagrams for the simply supported aluminum panel at moderately high dynamic loading, $\lambda = 1100.0$, and high dynamic loading, $\lambda = 2500.0$, respectively. Apparently, at $\lambda = 1100.0$,

Table 2 Material properties, geometry, and boundary conditions of panels under study

Panel	Material	Geometry $a \times b \times h$, in. (cm)	Lamination	Boundary condition	E_{11}, Msi (GPa)	E_{22}, Msi (GPa)	G_{12}, Msi (GPa)	ν_{12}	Density, lb · s^2/in.^{4} (kg/m^3)	Thermal expansion coefficients α_1/°F(°C)	α_2/°F(°C)
1	Al	$12 \times 12 \times 0.05$ ($30.5 \times 30.5 \times 0.13$)	NA	Simply supported	10.0 (68.9)	10.0 (68.9)	3.84 (26.5)	0.3	2.6×10^{-4} (2764)	1.25×10^{-5} (2.25×10^{-5})	1.25×10^{-5}
2	B/Al	$12 \times 12 \times 0.04$ ($30.5 \times 30.5 \times 0.10$)	[0]	Simply supported	31.0 (214)	20.0 (138)	8.40 (58)	0.27	2.46×10^{-4} (2615)	3.22×10^{-6} (5.80×10^{-6})	1.06×10^{-5} (1.91×10^{-5})
3	B/Al	$12 \times 12 \times 0.04$	[0/90]	Simply supported	31.0	20.0	8.40	0.27	2.46×10^{-4}	3.22×10^{-6}	1.06×10^{-5}
4	Gr/Ep	$12 \times 12 \times 0.048$	$[0/45/-45/90]_s$	Clamped	22.5	1.17	0.66	0.22	1.458×10^{-4}	-0.04×10^{-6}	1.67×10^{-5}
5	Gr/Ep	$12 \times 12 \times 0.048$ ($30.5 \times 30.5 \times 0.12$)	$[0/45/-45/90]_s$	Simply supported	22.5 (155)	1.17 (8.1)	0.66 (4.6)	0.22	1.458×10^{-4} (1550)	-0.04×10^{-6} (-0.07×10^{-6})	1.67×10^{-5} (3.0×10^{-5})
6	Gr/Ep	$15 \times 12 \times 0.048$ ($38.1 \times 30.5 \times 0.12$)	$[0/45/-45/90]_s$	Clamped	22.5	1.17	0.66	0.22	1.458×10^{-4}	-0.04×10^{-6}	1.67×10^{-5}

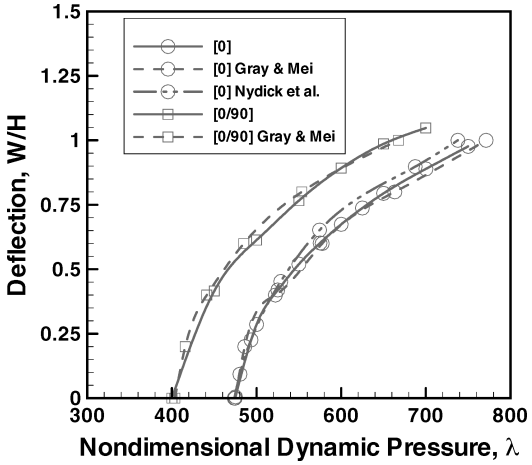

Fig. 1 Comparison of LCO amplitudes of simply supported B/Al square panels at hypersonic airflow.

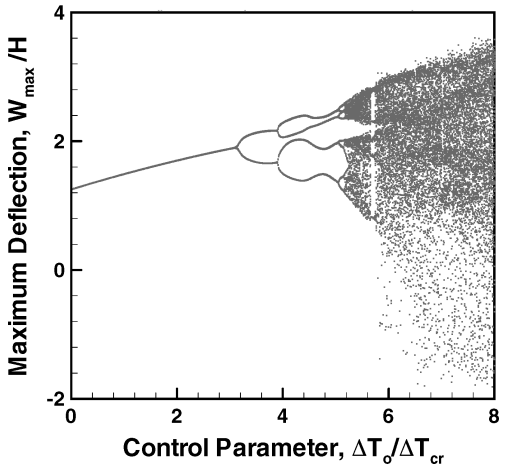

Fig. 2 Bifurcation diagram for a simply supported, 12 × 12 × 0.05 in. aluminum panel at $\lambda = 1100.0$: $C_a = 0.10$, $M_r = 0.05$, $\lambda = 1100$, and $T_1 = 0$.

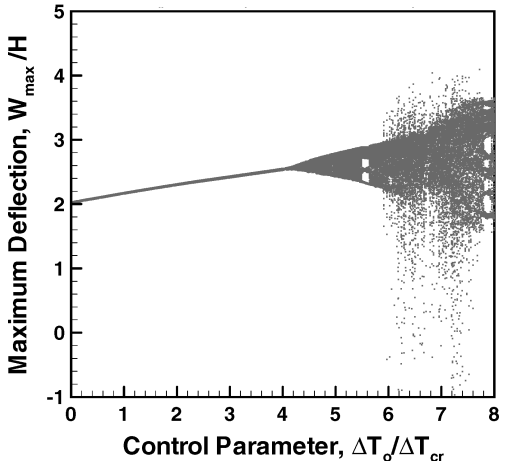

Fig. 3 Bifurcation diagram for a simply supported, 12 × 12 × 0.05 in. aluminum panel at $\lambda = 2500.0$: $C_a = 0.10$, $M_r = 0.05$, $\lambda = 2500$, and $T_1 = 0$.

the panel takes a pitchfork bifurcation route to evolve into chaos. The route is symbolized with a cascade of pitchfork bifurcations that finally lead to fully developed chaotic motions as temperature increases. However, at $\lambda = 2500.0$, the evolution of chaos does not show obvious pitchfork bifurcations. As shown in Fig. 3, the period-one LCO gradually develops into chaos at a certain temperature level in the bifurcation diagram. The deterministic chaos diagnosis tool, the Lyapunov exponent, is also introduced to assist in the identification of commencement of chaos. The bifurcation characteristics shown in Figs. 2 and 3 were found to be typical in all panels studied.

C. Flutter of Orthotropic Panels

One important issue for the finite element modal formulation is the mode selection strategy. The essence of this issue is that any modal reduction technique assumes an approximation to the true solution of the physical problem. A good selection method for the modes to use leads to an accurate simulation. Structural vibration is usually dominated by low-frequency modes. For a fluttering panel at hypersonic flow, the airflow provides the energy source for activating high-order modes so that they may play a more significant role.

With the importance of the selection of proper modes noted, a systematic mode filtering scheme is developed and adopted in this study. The influential modes are identified on checking of corresponding mode participation factors.[33,39] The basic steps include the following. 1) Choose several representative flow speed ranges and temperatures. The simulated LCO amplitudes are then examined. 2) Use the first 20 (or more) modes of lowest frequencies for numerical integration. 3) Record the LCO amplitudes for each case (specific flow speed and temperature). 4) Examine the modal participation factors for each mode and discard modes with a contribution less than certain level (less than 1% in the present study). Introduce more modes (to make up the total number to be 20), which are of higher order than the examined 20 modes, and repeat the numerical integration. 5) Record the LCO amplitudes and compare with previous results to check LCO amplitudes convergence. 6) If the LCO amplitudes for all cases have converged, the modes used for most recent step should be the final choice. If not converged, go to step 4. The procedure can be modified to a 25-mode base or 30-mode base if necessary.

For the single-layer B/Al panel, as the conclusion of mentioned mode-filtering procedure, up to 13 candidate modes are required to achieve a converged LCO solution. The mode shapes of these 13 modes were plotted after an eigenanalysis. The plots revealed that the first 7 flow direction modes, that is, modes (1, 1), (2, 1), . . . , (7, 1), and modes (2, 3), (3, 3), (1, 3), (4, 3), (3, 5), and (5, 3) are among the 13 candidate modes. Attention must be paid when comparing this mode selection conclusion with that by Nydick et al.[12] because different panel material and geometry are used. The conclusion drawn here serves better as an advice rather than as a general rule. The 13 modes are selected for further numerical integration experiments. A finite element discretization mesh convergence study was conducted,[33] and it concluded that a 12×8 mesh is sufficiently accurate for converged LCO amplitude.

The first numerical example is dedicated to investigate the effects of each nonlinear aerodynamic term in the full-form piston theory on LCO amplitudes. When the aerodynamic pressure expression given in Eq. (1) is expanded, there are totally seven nonlinear aerodynamic terms. Four of these seven terms, $C_{2x}(\partial w/\partial x)^2$, $C_{2t}(\partial w/\partial t)^2$, $C_{3x}(\partial w/\partial x)^3$, and $C_{3t}(\partial w/\partial t)^3$, possess specific physical meaning because $\partial w/\partial t$ is the panel velocity and $\partial w/\partial x$ is the slope. Therefore, the influences of these four terms on panel LCO are highlighted for a clear physical understanding. The roles of the six switch variables are very lucid: Switch on/off the influence of corresponding terms. Table 3 demonstrates the influence of the nonlinear aerodynamic terms. Case 1 and case 4 correspond to the first- and second-order piston theories, respectively. Several conclusions can be drawn on basis of a careful review of all results: 1) At low or moderately high λ, LCO amplitudes obtained using second-order piston theory notably differ from those using first-order piston theory; however, almost agree with those obtained using third-order piston theory. 2) At high λ, LCO amplitudes obtained from the first-, second-, and third-order theories are all different. 3) At all λ value ranges, the term $(\partial w/\partial x)^2$ causes more difference than $(\partial w/\partial t)^2$, and $(\partial w/\partial x)^3$ is more influential than $(\partial w/\partial t)^3$. The first conclusion was also observed by Eastep and McIntosh[9] and Gray and Mei.[6] The overwhelming effect of term $(\partial w/\partial x)^2$ against $(\partial w/\partial t)^2$ was also addressed by these researchers. The second conclusion is believed to be revealed for the first time and is specific to high values of nondimensional dynamic pressure, which is highly possible in the

Table 3 Effects on limit cycle amplitude by neglecting higher-order terms in aerodynamic piston theory for single layer B/Al panel with uniform temperature distribution ($\Delta T_0/\Delta T_{cr} = 2.0$)

							Dynamic pressure λ				
Case	C_{1t}	C_{1x}	C_{2t}	C_{2x}	C_{3t}	C_{3x}	500	1000	1500	2000	2500
1	1	1	0	0	0	0	1.0453	1.6218	1.9529	2.2010	2.3865
2	1	1	1	0	0	0	1.0453	1.6218	1.9529	2.2010	2.3865
3	1	1	0	1	0	0	1.0866	1.6787	2.0767	2.2093	2.6430
4	1	1	1	1	0	0	1.0849	1.6591	2.0487	2.2063	2.4645
5	1	1	1	1	1	0	1.0849	1.6591	2.0487	2.2063	2.4645
6	1	1	1	1	0	1	1.0838	1.6585	2.0633	2.2054	2.4733
7	1	1	1	1	1	1	1.0838	1.6587	2.0637	2.2008	2.4730

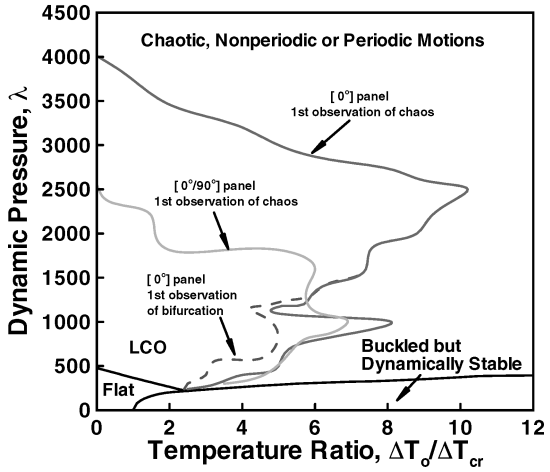

Fig. 4 Motion map for simply supported, [0] and [0/90], 12 × 12 × 0.04 in. B/Al panels: $M_r = 0.05$, $C_a = 0.1$, and $T_1 = 0.0$.

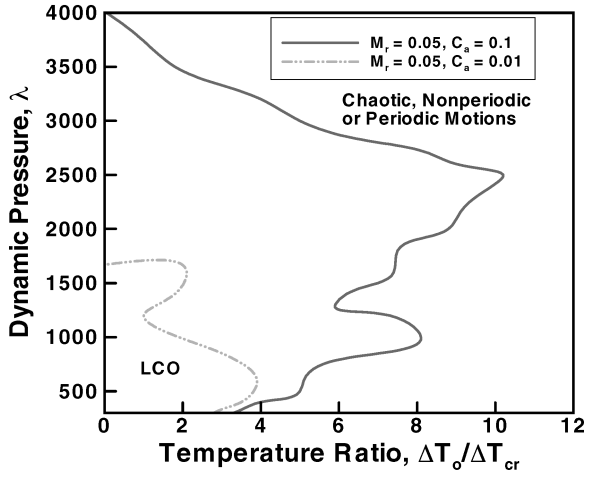

a) $M_r = 0.05$

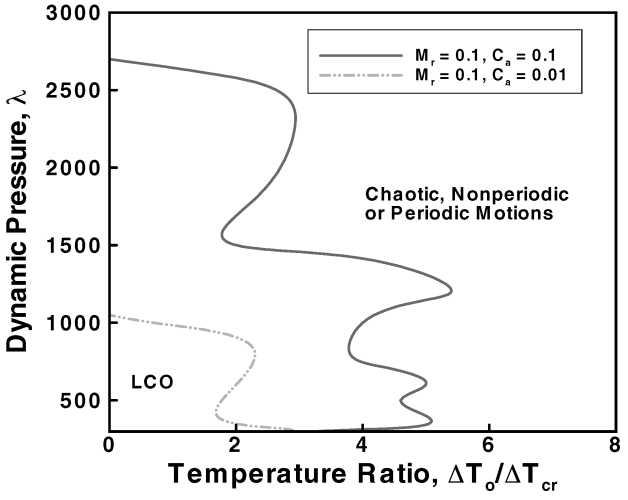

b) $M_r = 0.1$

Fig. 5 Effects of aerodynamic parameters on LCO region boundary of a simply supported, [0], 12 × 12 × 0.04 in. B/Al panel.

circumstance of hypersonic flow. A physical understanding of the third conclusion is that the slope-related nonlinear terms, $(\partial w/\partial x)^2$ and $(\partial w/\partial x)^3$, when considered, will affect the geometry boundary of the flow, hence the pressure distribution, whereas the velocity related terms, $(\partial w/\partial t)^2$ and $(\partial w/\partial t)^3$, do not have such effects. When all three conclusions are observed, it is suggested that full form of third-order piston theory should be used in studying flutter response of panels at hypersonic airflow.

It is well accepted that the stability boundaries of a fluttering panel can be established by applying linear aerodynamic theory. Many efforts have been made to show a stability plot that marks regions of possible panel configurations and motions in supersonic flow, such as Fig. 3 of Dowell,[40] Figs. 5.22–5.24 of Xue,[41] and Fig. 1 of Zhou et al.[31] All such plots are helpful for supersonic vehicle designers because, with information provided in such a map, care can be taken to avoid operation of the vehicle in dangerous parameter regions. However, because of the limitation of linear aerodynamic theory, the bounds of the region for LCO are usually either not well-defined or incomplete. The reason for defining the boundary of the LCO regions stems from the objective of studying LCO. One crucial concern in panel flutter designs is the fatigue life estimation.[6,41] Fatigue failure of skin panels could be caused by flutter, LCO, or chaotic motion. There exist different fatigue life evaluation algorithms for LCO or chaotic motions, and their usage domains are object oriented.[42]

Figure 4 shows a motion map for the simply supported, single-layer and cross-ply B/Al panels. The critical buckling temperature ΔT_{cr} for the [0] panel is 2.2186°F (1.2326°C). In Fig. 4, the boundaries that distinguish the flat and stable region and LCO region and buckled but dynamically stable region, as well as the upper bound of the buckled panel region, are determined by use of a finite element supersonic flutter analysis program used previously in Ref. 43. The rest of the bounds for LCO region is then obtained by direct numerical integration using the finite element time-domain modal formulation for hypersonic flutter developed in present work.

There are two aerodynamic parameters pertinent to current study subject to changes induced by various flight situations: M_r $(= M_\infty r)$, which is the product of Mach number and panel geometry constant $r = h/a$, and C_a, which is the aerodynamic damping coefficient. According to Dowell,[4] the typical aerodynamic damping ranges from $C_a = 0.01$ to 0.1. The flow parameter M_r was first used in hypersonic panel flutter analysis by Eastep and McIntosh,[9] and the typical values are $M_r = 0.05$ and 0.1 for low and high Mach numbers. The influence of M_r and aerodynamic damping on the LCO region boundary of the single-layer panel is investigated with various combinations of aforementioned typical values. Results are shown in Fig. 5a and 5b. As can be seen from Fig. 5, increasing M_r will result in decrease of the area for LCO. Also it is seen that

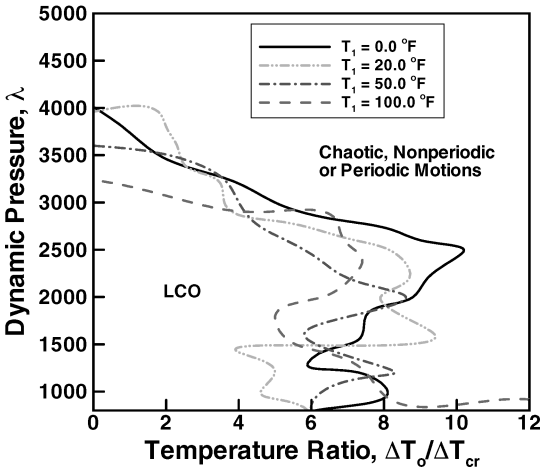

Fig. 6 Effects of temperature gradient on LCO region boundary of a simply supported, [0], 12 × 12 × 0.04 in. B/Al panel.

aerodynamic damping has a more significant effect on LCO region bounds. In summary, when $M_r = 0.05$ and $C_a = 0.1$, the area of the LCO region is the largest, and when $M_r = 0.1$ and $C_a = 0.01$, the LCO region is the smallest of all four cases.

Temperature gradient T_1 introduces thermal moments that cause bending to the plate. Generally speaking, the bending induced by thermal moments exerts a stiffening effect on the panel, whereas the thermal expansion due to the elevated average temperature T_0 plays a softening role. Coexistence of these two conflicting actions causes noticeable changes to the stability boundary of a fluttering panel, as discussed in Cheng et al.[43] It is concluded that temperature gradient improves the panel motion with the raising of the linear flutter stability boundary and the delaying of its descending as average temperature increases. It is of interest to investigate the influence of temperature gradient on the boundary of the LCO region. Figure 6 is the motion map for the single layer B/Al panel with three representative temperature gradient values, $T_1 = 20$, 50, and 100°F over a 0.040-in. panel thickness. Note from Fig. 6 that a tendency of lowering and broadening LCO region boundary as temperature gradient increases can be observed from the comparisons of boundary curves.

D. Flutter of Laminated Composite Panels

High thermal performance and light weight are among the principal goals for design choices of advanced materials for flight vehicle surface panels. Besides the metal matrix composites, with B/Al as a special example, polymeric-based composite materials also have been used extensively in aerospace designs. As a representative of this family of composites, the Gr/Ep laminated composite is among the most commonly used material in aerospace engineering. The aeroelastic performances of Gr/Ep panels are investigated as examples to show the effects of hypersonic airflow and thermal loadings.

Three Gr/Ep panels, a clamped square, a simply supported square, and a clamped rectangular panel of aspect ratio 1.25, are taken into consideration. The purpose is to investigate the influence of different supporting conditions and aspect ratios. Figure 7 shows the comparison of the motion maps for the three panels. Note that the temperature axis of Fig. 7 is the absolute temperature because the thermal buckling temperatures for these panels are different: For the clamped square panel, $\Delta T_{cr} = 54.55$°F (30.31°C); for the simply supported square panel, $\Delta T_{cr} = 19.71$°F (10.95°C); and for the rectangular panel, $\Delta T_{cr} = 36.48$°F (20.27°C). An 12×8 mesh is used for all three panels. The mode selection study concludes that 14 modes are required to achieve converged LCO solutions for clamped square and rectangular panels, whereas the simply supported panel case needs 13 modes. A few remarks about the three designs follow. 1) If the thermal performance is the only concern, that is, aerodynamic loading is neglectable, the clamped square panel is the best choice because of its high ΔT_{cr}. 2) If linear flutter stability boundary with thermal effects is the primary concern, the clamped rectangular panel is the best choice because it has the biggest stable region in the motion map. 3) If thermal effects, linear stability boundary, and the area of LCO region are considered together, the clamped square panel is relatively better than the other two designs because it has a larger area of LCO region and the linear stability boundary is moderately high. 4) None of the three designs is immune from chaotic motion when the temperature increase is higher than 180°F (100°C), even if the dynamic pressure is low.

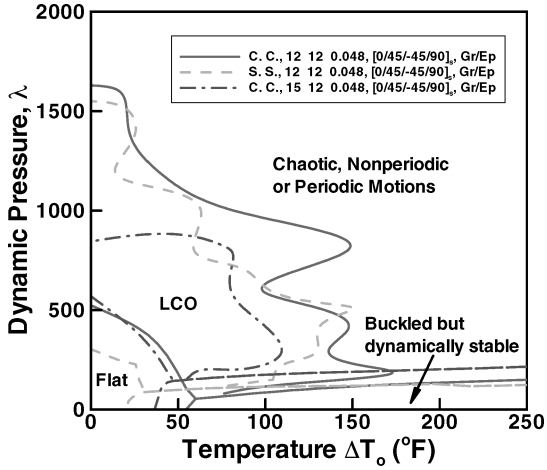

Fig. 7 Comparison of motion maps for Gr/Ep panels.

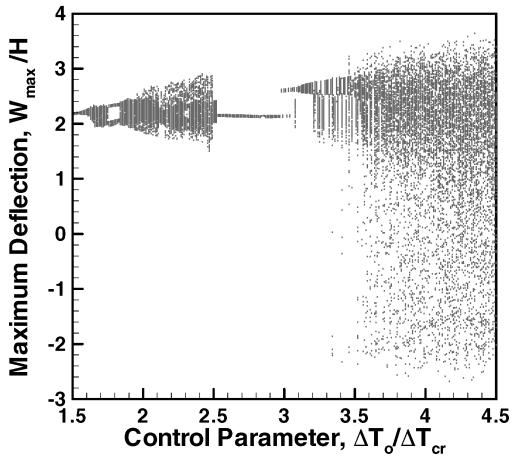

a) Bifurcation diagram

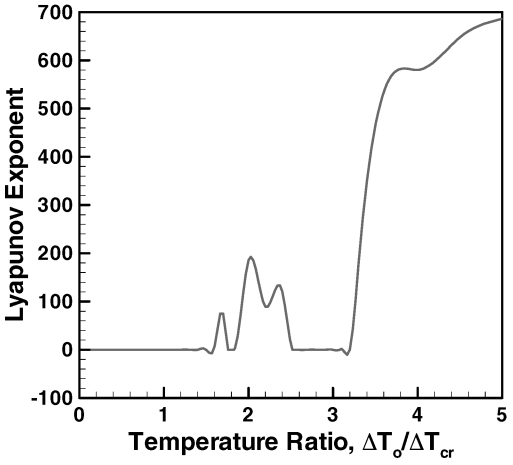

b) Lyapunov exponent

Fig. 8 Evolution of chaos for a clamped Gr/Ep square panel at $\lambda = 1000$: $C_a = 0.10$, $M_r = 0.05$, $\lambda = 1000$, and $T_1 = 0$.

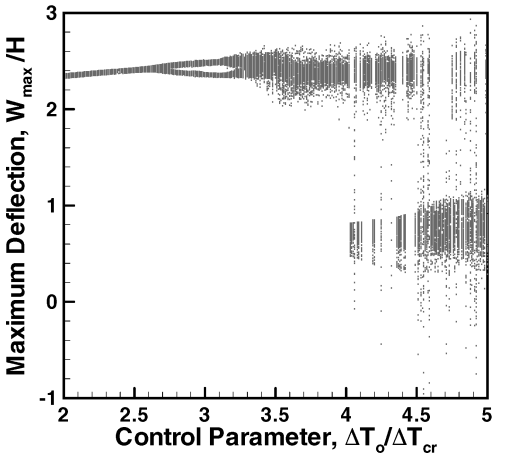

a) Bifurcation diagram

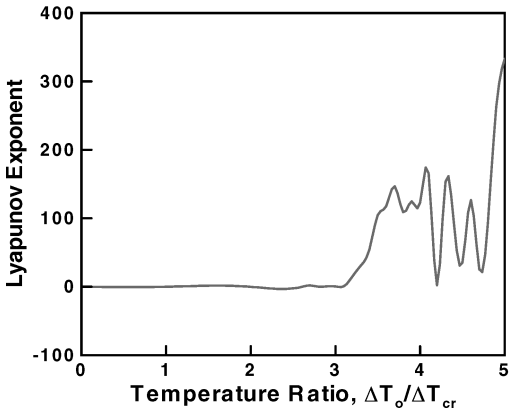

b) Lyapunov exponent

Fig. 9 Evolution of chaos for a simply supported Gr/Ep square panel at $\lambda = 1000$: $C_a = 0.10$, $M_r = 0.05$, $\lambda = 1000$, and $T_1 = 0$.

Also observe that the entry into chaos is affected by supporting conditions. Figures 8 and 9 show the different routes to chaos for clamped square panel and simply supported square panel through bifurcation diagrams and Lyapunov exponents. For the clamped panel, the periodic LCO suddenly bursts into chaos, and this intermittency yields to period-one motion as temperature increases. Further increasing temperature leads to fully developed chaos. The chaotic motion of simply supported panel develops in a mild way: Period-one motion bifurcates into period-two motion, then intermittency appears in the bifurcation diagram. In fact, it is typically observed in the present hypersonic panel flutter study that route to pitchfork bifurcations is found when the dynamic pressure is low or moderately high and that intermittency is more or less related to high dynamic pressures. Thus, in an engineering sense, the pitchfork bifurcation route is mild, and the intermittency way is violent. As Moon[35] described it, "The period-doubling model for the route to chaos is an elegant, aesthetic model and has been described in many popular articles." This elegant pitchfork bifurcation route would appear to be a potential good aim for hypersonic flight vehicle designers because a sudden burst of chaos without a precursor is more difficult to predict and prevent.

Conclusions

The primary objective of this work is to develop a finite element time-domain modal formulation that could be applied to analyze the panel flutter problems for high supersonic/hypersonic flight vehicles. The modal formulation was aimed to save computational cost by reducing the number of equations dramatically without losing much accuracy. From a practical point of view, the issue of mode selection must be clarified for any modal reduction approach. The modes for finite element procedures are from eigenanalysis and depend on the complexity of material property. The edge support conditions cause a great deal of confusions in mode selection. The mode filtering procedure proposed in present work is an initial attempt to provide a systematic means to screen out the influential modes based on the well-defined modal participation factor concept.

Chaos is inevitable if there is or is not thermal loading. With the efficient finite element modal formulation, it is easier to detect and inspect chaos in many ways, such as time history, phase plane plot, Poincaré map, and bifurcation diagram. The largest Lyapunov exponent can be evaluated based on data from direct time integration. All of these mathematical tools are applied to establish the motion maps for orthotropic panels and composite panels. It is observed that a fluttering panel typically takes either of two typical routes to evolve into chaos: the period-doubling (associated with cascade of pitchfork bifurcations) route and the intermittent (sudden burst of chaos followed by periodic LCOs) transitions route. A few more conclusions can be drawn from the numerical study examples.

1) At high dynamic pressure, the slope pertinent cubic term, $(\partial w/\partial x)^3$, in the third-order piston theory is of importance.

2) The effect of aerodynamic damping on the area of LCO region is significant; high damping gives large LCO region.

3) Existence of temperature gradients will lower the upper boundary (dynamic pressure) of LCO region and slightly defer the onset of chaos to high average temperature.

4) If critical thermal buckling temperature, linear flutter stability boundary, and area of LCO region in the motion map are all of concern, the clamped square Gr/Ep panel behaves better than the simply supported square panel and the clamped rectangular panel with an aspect ratio of 1.25.

References

[1]Fung, Y. C., "A Summary of the Theories and Experiments on Panel Flutter," Guggenheim Aeronautical Lab., U.S. Air Force Office of Scientific Research, AFOSR TN 60-224, California Inst. of Technology, Pasadena, CA, May 1960.

[2]Johns, D. J., "The Present Status of Panel Flutter," AGARD Rept. 484, Oct. 1984.

[3]Johns, D. J., "A Survey on Panel Flutter," AGARD Advisory Rept. 1, Nov. 1965.

[4]Dowell, E. H., "Panel Flutter: A Review of the Aeroelastic Stability of Plates and Shells," *AIAA Journal*, Vol. 8, No. 3, 1970, pp. 385–399.

[5]Mei, C., Abdel-Motagaly, K., and Chen, R., "Review of Nonlinear Panel Flutter at Supersonic and Hypersonic Speeds," *Applied Mechanics Reviews*, Vol. 52, No. 10, 1999, pp. 321–332.

[6]Gray, C. E., and Mei, C., "Large Amplitude Finite Element Flutter Analysis of Composites Panels in Hypersonic Flow," *AIAA Journal*, Vol. 31, No. 6, 1993, pp. 1090–1099.

[7]McIntosh, S. G., Jr., "Theoretical Considerations of Some Nonlinear Aspects of Hypersonic Panel Flutter," Dept. of Aeronautics and Astronautics, Final Rept., NASA Grant NGR 05-020-102, Stanford Univ., Stanford, CA, Nov. 1974.

[8]McIntosh, S. C., Jr., "Effect of Hypersonic Nonlinear Aerodynamic Loading on Panel Flutter," *AIAA Journal*, Vol. 11, No. 1, 1973, pp. 29–32.

[9]Eastep, F. E., and McIntosh, S. C., Jr., "Analysis of Nonlinear Panel Flutter and Response Under Random Excitation or Nonlinear Aerodynamic Loading," *AIAA Journal*, Vol. 9, No. 3, 1971, pp. 411–418.

[10]Gray, C. E., Jr., and Mei, C., "Finite Element Method for Large-Amplitude Two-Dimensional Panel Flutter at Hypersonic Speeds," *AIAA Journal*, Vol. 29, No. 2, 1991, pp. 290–298.

[11]Bein, T., Friedmann, P., Zhong, X., and Nydick, I., "Hypersonic Flutter of a Curved Shallow Panel with Aerodynamic Heating," AIAA Paper 93-1318, April 1993.

[12]Nydick, I., Friedmann, P. P., and Zhong, X., "Hypersonic Panel Flutter Studies on Curved Panels," *AIAA 36th Structures, Structural Dynamics, and Materials Conference*, AIAA, Washington, DC, 1995, pp. 2995–3011.

[13]Thuruthimattam, B. J., Friedmann, P. P., McNamara, J. J., and Powell, K. G., "Aeroelasticity of a Generic Hypersonic Vehicle," AIAA Paper 2002-1209, April 2002.

[14]Chandiramani, N. K., Plaut, R. H., and Librescu, L. I., "Nonperiodic Flutter of a Buckled Composite Panel," *Sādhanā*, Vol. 20, Pts. 2-4, 1995, pp. 671–689.

[15]Chandiramani, N. K., Plaut, R. H., and Librescu, L. I., "Non-Linear Flutter of a Buckled Shear Deformable Composite Panel in a High-Supersonic Flow," *International Journal of Non-Linear Mechanics*, Vol. 30, No. 2, 1995, pp. 149–167.

[16]Chandiramani, N. K., and Librescu, L. I., "Flutter of Geometrically-Imperfect Shear-Deformable Laminated Flat Panels Using Non-Linear Aerodynamics," *Journal of Sound and Vibration*, Vol. 192, No. 1, 1996, pp. 79–100.

[17]Sri Namachchivaya, N., and Lee, A., "Dynamics of Nonlinear Aeroelastic Systems," *Symposium of Fluid–Structure Interaction, Aeroelasticity, Flow-Induced Vibration and Noise*, Vol. 3, American Society of Mechanical Engineers, Fairfield, NJ, 1976, pp. 165–174.

[18]Chen, P. C., and Liu, D. D., "A Harmonic Gradient Method for Unsteady Supersonic Flow Calculations," *Journal of Aircraft*, Vol. 22, No. 5, 1985, pp. 371–379.

[19]Chavez, F. R., and Liu, D. D., "Unsteady Unified Hypersonic/Supersonic Method for Aeroelastic Applications Including Wave/Shock Interaction," *AIAA Journal*, Vol. 33, No. 6, 1995, pp. 1090–1097.

[20]Liu, D. D., Yao, Z. X., Sarhaddi, D., and Chavez, F. R., "From Piston Theory to a Unified Hypersonic–Supersonic Lifting Surface Method," *Journal of Aircraft*, Vol. 34, No. 3, 1997, pp. 304–312.

[21]Goldstein, M. E., "Boundary-Layer Effect in Panel Flutter," *AIAA Journal*, Vol. 13, No. 9, 1975, pp. 1247–1249.

[22]Muhlstein, L., Jr., Gaspers, P. A., Jr., and Riddle, D. W., "An Experimental Study of the Turbulent Boundary Layer on Panel Flutter," NASA TN-D-4486, March 1968.

[23]Gaspers, P. A., Jr., Muhlstein, L., Jr., and Petroff, D. N., "Further Experimental Results on the Influence of the Turbulent Boundary Layer on Panel Flutter," NASA TN-D-5798, May 1970.

[24]Gordnier, R. E., and Visbal, M. R., "Development of a Three-Dimensional Viscous Aeroelastic Solver for Nonlinear Panel Flutter," *Journal of Fluids and Structures*, Vol. 16, No. 4, 2002, pp. 497–527.

[25]Gordnier, R. E., and Visbal, M. R., "Computation of Three-Dimensional Nonlinear Panel Flutter," AIAA Paper 2001-0571, Jan. 2001.

[26]Crandall, S. H., and Zhu, W. Q., "Random Vibration: A Survey of Recent Developments," *Journal of Applied Mechanics*, Vol. 50, 1983, pp. 953–962.

[27]Abdel-Motagaly, K., Duan, B., and Mei, C., "Nonlinear Response of Composite Panels Under Combined Acoustic Excitation and Aerodynamic Pressure, " *AIAA Journal*, Vol. 38, No. 9, 2000, pp. 1534–1542.

[28]Selvam, R. P., Qu, Z., and Zheng, Q., "Three-Dimensional Nonlinear Panel Flutter at Supersonic Euler Flow," AIAA Paper 2002-1485, April 2002.

[29]Green, P. D., and Killey, A., "Time Domain Dynamic Finite Element Modeling in Acoustic Fatigue Design," *Proceedings of the 6th International Conference on Structural Dynamics*, Inst. of Sound and Vibration Research, Univ. of Southampton, Southampton, England, U.K., 1997, pp. 1007–1026.

[30]Robinson, J. H., "Finite Element Formulation and Numerical Simulation of the Large Deflection Random Vibration of Laminated Composite Plates," M.S. Thesis, Aerospace Engineering Dept., Old Dominion Univ., Norfolk, VA, Dec. 1990.

[31]Zhou, R. C., Xue, D. Y., and Mei, C., "Finite Element Time Domain-Modal Formulation for Nonlinear Flutter of Composite Panels," *AIAA Journal*, Vol. 32, No. 10, 1994, pp. 2044–2052.

[32]Ashley, H., and Zartarian, G., "Piston Theory—A New Aerodynamic Tool for the Aeroelastician," *Journal of Aeronautical Science*, Vol. 23, No. 10, 1956, pp. 1109–1118.

[33]Cheng, G. F., "Finite Element Modal Formulation for Panel Flutter at Hypersonic Speeds and Elevated Temperatures," Ph.D. Dissertation, Aerospace Engineering Dept., Old Dominion Univ., Norfolk, VA, Dec. 2002.

[34]Bathe, K. J., *Finite Element Procedures*, Prentice Hall, Upper Saddle River, NJ, 1996, Chap. 9.

[35]Moon, F. C., *Chaotic and Fractal Dynamics—An Introduction for Applied Scientists and Engineers*, Wiley, New York, 1992, Chaps. 2 and 5.

[36]Dowell, E. H., "Observation and Evolution of Chaos in an Autonomous System," *Journal of Applied Mechanics*, Vol. 51, 1984, pp. 664–673.

[37]Wolf, A., Swift, J. B., Swinney, H. L., and Vastano, J. A., "Determining Lyapunov Exponents from a Time Series," *Physica*, Vol. 16D, 1985, pp. 285–317.

[38]Dowell, E. H., "Nonlinear Oscillation of a Fluttering Plate I," *AIAA Journal*, Vol. 4, No. 7, 1966, pp. 1267–1275.

[39]Abdel-Motaglay, K., Chen, R., and Mei, C., "Nonlinear Flutter of Composite Panels Under Yawed Supersonic Flow Using Finite Elements," *AIAA Journal*, Vol. 37, No. 9, 1999, pp. 1025–1032.

[40]Dowell, E. H., "Flutter of a Buckled Plate as an Example of Chaotic Motion of a Deterministic Autonomous System," *Journal of Sound and Vibration*, Vol. 85, No. 3, 1982, pp. 333–344.

[41]Xue, D. Y., "A Finite Element Frequency Domain Solution of Nonlinear Panel Flutter with Temperature Effects and Fatigue Life Analysis," Ph.D. Dissertation, Aerospace Engineering Dept., Old Dominion Univ., Norfolk, VA, Oct. 1991.

[42]Dhainaut, J. M., "Nonlinear Response and Fatigue Estimation of Surface Panels to White and Non-White Gaussian Random Excitations," Ph.D. Dissertation, Aerospace Engineering Dept., Old Dominion Univ., Norfolk, VA, Dec. 2001.

[43]Cheng, G. F., Lee, Y. Y., and Mei, C., "Flow Angle, Temperature, and Aerodynamic Damping on Supersonic Panel Flutter Stability Boundary," *Journal of Aircraft*, Vol. 40, No. 2, 2003, pp. 248–255; also AIAA Paper 2002-1285, April 2002.

E. Livne
Associate Editor